Strangeness Production in Nuclear Matter and Expansion Dynamics

V.D. Toneev[a,b], E.G. Nikonov[a,b],
B. Friman[a], W. Nörenberg[a], K. Redlich[c,d]

[a] Gesellschaft für Schwerionenforschung GSI,
D–64291 Darmstadt, Germany
[b] Joint Institute for Nuclear Research, 141980 Dubna,
Moscow Region, Russia
[c] Fakultät für Physik, Universität Bielefeld,
D–33501 Bielefeld, Germany
[d] Institute of Theoretical Physics, University of Wrocław,
PL–50204 Wrocław, Poland

Abstract

Thermodynamical properties of hot and dense nuclear matter are analyzed and compared for different equations of state (EoS). It is argued that the softest point of the equation of state and the strangeness separation on the phase boundary can manifest themselves in observables. The influence of the EoS and the order of the phase transition on the expansion dynamics of nuclear matter and strangeness excitation function is analyzed. It is shown that bulk properties of strangeness production in A–A collisions depend only weakly on the particular form of the EoS. The predictions of different models are related with experimental data on strangeness production.

1 Introduction

The quest for the deconfinement transition, the phase transition from a confined hadronic phase to a deconfined quark–gluon phase (the so called quark–gluon plasma, QGP), remains a major challenge in strong interaction physics [1]. Over the past two decades a lot of effort has gone into the exploration of this transition and its possible manifestations in relativistic heavy ion collisions, in neutron stars as well as in the early universe. Relativistic heavy ion collisions offers a unique opportunity to reach states with temperatures and energy densities exceeding the critical values, $T_c \sim 170\ MeV$ and $\varepsilon_c \sim 0.6\ GeV/\mathrm{fm}^3$, specific for the deconfinement phase transition [2]. Thus, it is likely that color degrees of freedom play an important role already at SPS and RHIC energies [3]. Various signals for the formation of a quark–gluon plasma in such collisions have been discussed and probed in experiments [1, 4].

Enhanced production of strangeness relative to proton–proton and proton–nucleus collisions was one of the conjecture signals of the quark–gluon plasma formation in heavy ion collisions [5]. The original idea behind the strangeness enhancement is that strange and antistrange quarks are easily created in a quark–gluon plasma, while in the hadronic phase strangeness production is suppressed. The dominant reaction in the plasma is $gg \rightarrow s\bar{s}$. Furthermore, since the strange quark mass is not larger than T_c, one expects the strange degrees of freedom to equilibrate in the quark–gluon plasma. Although, a heavy ion collision at high energies is a highly non–equilibrium process, the hadron yields (including strange particles) measured in the energy range from SIS to RHIC [6, 7, 8, 9, 10] are remarkably well described in the thermal model assuming chemical equilibrium at freeze out. This indicates that collective effects play an important role in the production of strangeness. On the other hand, elaborate microscopic transport models do not provide a quantitative explanation of the excitation functions for strange particles in this energy range. In the hadron string dynamics model [11] one finds a too small K^+/π^+ ratio around AGS energies, while in RQMD [12] the yield is overestimated at SIS and too small at SPS energies.

The aim of this paper is to explore global effects of strangeness production in hot and dense nuclear matter within a collective approach. Our starting point is an equation of state (EoS) with a deconfinement phase transition. Since strangeness is conserved at the time scales relevant for heavy ion collisions, a strangeness chemical potential is introduced. We examine

various phenomenological models for the equation of state, which differ in the order of the deconfinement phase transition: a first order transition (the two–phase bag model), a crossover–type transition (the statistical mixed–phase model) and no phase transition (pure hadronic models). The consequences of strangeness separation and softening of the equation of state are discussed. Furthermore, the manifestation of the order of the deconfinement phase transition in the expansion dynamics and the bulk strangeness production is studied. The predictions obtained with different equations of state are related with experimental excitation functions for relative strange particle abundances.

2 Modelling the equation of state of strongly interacting matter

The EoS of strongly interacting matter can in general be obtained by first principal calculations within lattice gauge theory [13]. The thermodynamics and the order of the phase transition in QCD is rather well established for two and three light quark flavour in lattice calculations. However, the physically relevant situation of two light (u,d) and a heavy (s) quark is still not well described within lattice approach. In particular, the existence of a phase transition and its order in 2+1 flavour QCD is not yet known. In addition most of the lattice calculations are performed for vanishing net baryon number density. Only recently, first results on the EoS with non zero baryon chemical potential have been obtained on the lattice [14]. However, these studies have so far been performed with large quark masses which distort the physical EoS. Thus, lattice results can still not be used directly in physical applications.

Lacking lattice QCD results for the EoS at finite baryon density n_B with physically relevant values of the quark masses, a common approach is to construct a phenomenological equation of state for strongly interacting matter. This EoS should be constrained by existing lattice results and should also reproduce the two–phase structure of QCD. Here we construct different models for QCD thermodynamics and study their physical implications with particular emphasis on strangeness production and evolution in heavy ion collisions.

A recent analysis of the lattice EoS [15, 16], shows that in the low tem-

perature phase, hadrons and resonances are the relevant degrees of freedom. The hadron resonance gas, with a modified mass spectrum to account for the unphysical values of the quark masses used in the lattice calculations, was shown to reproduce the bulk thermodynamic properties of QCD, obtained on the lattice with different numbers of quark flavors as well as at finite and vanishing net baryon density [15, 16].

Lattice calculations show that, at very large temperature the thermodynamical observables approach the Stefan–Boltzmann limit of an ideal gas of quarks and gluons, both at finite as well as vanishing net baryon density. The remaining $\sim 20\%$ discrepancy at $T > 2T_C$ is understood by systematic contributions in self–consistent implementation of quasiparticle masses in the HTL–reassumed perturbative QCD [17]. To describe the thermodynamics near the phase transition additional model assumptions are necessary [18, 19].

From the above discussion it is clear that the most straightforward model for the EoS would be a non-interacting hadron resonance gas in the low temperature phase and ideal quark gluon–plasma in the color deconfined phase. These phases are matched at the phase transition boundary by means of the Gibbs phase equilibrium conditions. By construction, this approach yields a first order phase transition. Such an EoS with strange degrees of freedom has frequently been used in the literature [20, 21, 22, 23, 24, 25] and is also a standard input in hydrodynamic simulations of heavy ion collisions [26, 27]. However, in order to obtain a reasonable phase diagram one has to include short–range repulsive interactions between hadronic constituents. In general this can be realized by introducing short–range repulsion in a thermodynamically consistent approach [28, 29, 30, 31].

We note that according to Gibbs phase rule [32], the number of thermodynamic degrees of freedom that may be varied without destroying the equilibrium of a mixture of r phases, with n_c conserved charges is $\mathcal{N} = n_c + 2 - r$. For the hadron–quark deconfinement transition under consideration $r = 2$. If the baryon number is the only conserved quantity, $n_c = 1$ and $\mathcal{N} = 1$. Thus, the phase boundary is one–dimensional, i.e. a line. The Maxwell construction for a first order phase transition corresponds just to this case $r = 2$ and $n_c = 1$. When both the baryon number and strangeness are conserved ($n_c = 2$), one has $\mathcal{N} = 2$ and therefore the phase boundary is in general a surface. In such a system, a standard Maxwell construction is not possible [33].

To account for the uncertainties in the order of the phase transition in 2+1

4

flavour QCD and also for the deviation of the equation of state from an ideal gas near the deconfinement transition we employ the EoS of the mixed phase model [28, 29]. In this model it is assumed that unbound quarks and gluons may coexist with hadrons forming a homogeneous mixture. This model is thermodynamically consistent and reproduces the lattice EoS obtained in the pure gauge theory as well as in two flavour QCD. Furthermore, the order of the phase transitions in the mixed phase model depends on the strength of the interaction between the phases. In this approach we can study the importance of the order of the phase transition on strangeness production and on the evolution of heavy ion collisions.

In the following we discuss first the basic thermodynamical properties of these different models of the EoS and indicate relevant differences in their predictions.

2.1 Two–phase bag model

In the two–phase (2P) model [34], the deconfinement phase transition is determined by matching the EoS of a relativistic gas of hadrons and resonances, with repulsive interactions at short distances, to that of an ideal gas of quarks and gluons. The change in vacuum energy in the plasma phase is parameterized by a bag constant B. We work in the grand canonical ensemble and account for all hadrons with mass $m_j < 1.6 \ GeV$, including the strange particles and resonances with strangeness $s_j = \pm 1, \pm 2, \pm 3$. The density of particle species j is then

$$
\begin{aligned}
n_j(T, \mu_j) \equiv n_j(T, \mu_B, \mu_S) &= v \ n_j^{id}(T, \mu_B, \mu_S) \\
&= \frac{v \ g_j}{2\pi^2} \int_0^\infty dk \ k^2 \ f_j(k, T, \mu_B, \mu_S) \ ,
\end{aligned}
\tag{1}
$$

where

$$
f_j(k, T, \mu_B, \mu_S) = \left[exp\left(\frac{\sqrt{k^2 + m_j^2} - b_j \mu_B - s_j \mu_S}{T} \right) \pm 1 \right]^{-1}
\tag{2}
$$

is the momentum distribution function for fermions $(+)$ and bosons $(-)$ while g_j is the spin–isospin degeneracy factor. The chemical potential μ_j is related to the baryon (μ_B) and strangeness (μ_S) chemical potentials

$$
\mu_j = b_j \ \mu_B + s_j \ \mu_S \ ,
\tag{3}
$$

5

where b_j and s_j are the baryon number and strangeness of the particle. The quantity n_j^{id} corresponds to the number density of an ideal point–like hadron gas (IdHG). The factor

$$v \equiv v(T, \mu_B, \mu_S) = 1/[1 + \sum_j v_{0j} \; n_j^{id}(T, \mu_B, \mu_S)] \tag{4}$$

reduces the volume available for hadrons due to their short range repulsion determined by the eigenvolume $v_{0j} = (1/2)(4\pi/3)(2r_{0j})^3$ [32]. We choose the effective interaction radius $r_{0j} \sim 0.5\text{fm}$ for all hadrons. Following (1), the baryon density and strangeness in the hadronic phase can be expressed as

$$n_B^H = \sum_{j \in h} b_j \; n_j(T, \mu_B, \mu_S) \; , \tag{5}$$

$$n_S^H = \sum_{j \in h} s_j \; n_j(T, \mu_B, \mu_S) \tag{6}$$

where the sum is taken over all hadrons and resonances. Similarly, the energy density of species j is given by

$$
\begin{aligned}
\varepsilon_j(T, \mu_B, \mu_S) &= v \; \varepsilon_j^{id}(T, \mu_B, \mu_S) \\
&= \frac{v \; g_j}{2\pi^2} \int_0^\infty dk \; k^2 \sqrt{k^2 + m_j^2} \; f_j(k, T, \mu_B, \mu_S) \; . \tag{7}
\end{aligned}
$$

In early studies [34, 35], the excluded volume correction v was implemented in the same way for all thermodynamic quantities of the hadron gas, including the pressure

$$p^H(T, \mu_B, \mu_S) = \sum_{j \in h} p_j(T, \mu_B, \mu_S) \, , \tag{8}$$

where the partial pressures are given by

$$
\begin{aligned}
p_j(T, \mu_B, \mu_S) &= v \; p_j^{id}(T, \mu_B, \mu_S) \\
&= \frac{v \; g_j}{6\pi^2} \int_0^\infty dk \; \frac{k^4}{\sqrt{k^2 + m_j^2}} \; f_j(k, T, \mu_B, \mu_S) \; . \tag{9}
\end{aligned}
$$

However, this expansion for the pressure is not thermodynamically consistent with the charge (5-6) as well as the energy density (7). In Ref. [36] it was shown that, it is possible to account for a thermodynamically consistent

implementation of the excluded volume corrections. In this approach the pressure is given by that of an ideal gas with modified chemical potentials

$$p^H(T, \mu_B, \mu_S) = \sum_{j \in h} p_j^{id}(T, \tilde{\mu}_j) \tag{10}$$

where

$$\tilde{\mu}_j = b_j \, \mu_B + s_j \, \mu_S - v_{0j} \, p^H(T, \mu_B, \mu_S) \ . \tag{11}$$

The remaining thermodynamic quantities are obtained with the excluded volume correction given above by taking the corresponding derivatives of the pressure. Thus, in this approach all fundamental thermodynamic relations are fulfilled [36]. We shall refer to Eqs.(8,9) and Eqs.(10,11) as two–phase thermodynamically inconsistent (2PIN) and consistent (2PC) model, respectively. Note that such an equation of state may violate causality at high densities, because an extended rigid body is incompatible with the basic principles of relativity.

The QGP phase is described as a gas of non–interacting point-like quarks, antiquarks and gluons. The non–perturbative effects associated with confinement are described by the constant vacuum energy B. The pressure in the plasma is then given by

$$p^Q(T, \mu_B, \mu_S) = p_g(T) + \sum_{j \in q} p_j^{id}(T, \mu_B, \mu_S) - B \ , \tag{12}$$

where the gluon

$$p_g(T) = \frac{g_g \pi^2}{90} T^4 \qquad (g_g = 16) \tag{13}$$

and the quark pressure is obtained from Eq.(9) for u, d, s quarks and antiquarks. We use the quark masses $m_u = m_d = 5\text{MeV}$ and $m_s = 150\text{MeV}$ and the bag constant $B = (235\text{MeV})^4$ which yields a transition temperature $T_c \approx 160\text{MeV}$ in agreement with lattice calculations at $n_B = 0$ [13]. The energy density of the plasma phase

$$\varepsilon^Q(T, \mu_B, \mu_S) = \varepsilon_g(T) + \sum_{j \in q} \varepsilon_j^{id}(T, \mu_B, \mu_S) + B \ , \tag{14}$$

where the gluon contribution is given by

$$\varepsilon_g(T) = 3 \, p_g(T) = \frac{g_g \pi^2}{30} T^4 \tag{15}$$

7

and that of quark species j is obtained from Eq.(7) with $v = 1$. Analogously to Eqs.(5) and (6) the densities of the conserved charges in the QGP phase are :

$$n_B^Q = \sum_{j \in q} b_j \, n_j^{id}(T, \mu_B, \mu_S) \,, \tag{16}$$

$$n_S^Q = \sum_{j \in q} s_j \, n_j^{id}(T, \mu_B, \mu_S) \,. \tag{17}$$

The equilibrium between the plasma and the hadronic phase is determined by the Gibbs conditions for thermal $(T^Q = T^H)$, mechanical $(p^Q = p^H)$ and chemical $(\mu_B^Q = \mu_B^H, \ \mu_S^Q = \mu_S^H)$ equilibrium. At a given temperature T and baryon chemical potential μ_B the strange chemical potential μ_S is obtained by requiring that the net strangeness of the total system vanishes. Thus, for the total baryon density n_B the phase equilibrium requires that:

$$p^H(T, \mu_B, \mu_S) = p^Q(T, \mu_B, \mu_S) \,, \tag{18}$$

$$n_B = \alpha \, n_B^Q(T, \mu_B, \mu_S) + (1 - \alpha) \, n_B^H(T, \mu_B, \mu_S) \,, \tag{19}$$

$$0 = \alpha \, n_S^Q(T, \mu_B, \mu_S) + (1 - \alpha) \, n_S^H(T, \mu_B, \mu_S) \,, \tag{20}$$

where $\alpha = V_Q/V$ is the fraction of the volume occupied by the plasma phase. The boundaries of the coexistence region are found by putting $\alpha = 0$ (the hadron phase boundary) and $\alpha = 1$ (the plasma boundary).

As mentioned above, the Maxwell construction is not appropriate in a system where both baryon number and strangeness are conserved. To illustrate this, we first analyze an approximate form of the equation (17) for strangeness conservation. We retain only the main terms and drop those with $|s_j| > 1$:

$$\alpha \, (n_s - n_{\bar{s}}) = (1 - \alpha) \, (n_K + n_{\bar{\Lambda}} + n_{\bar{\Sigma}} - n_{\bar{K}} - n_\Lambda - n_\Sigma) \,. \tag{21}$$

In the Boltzmann approximation the densities may be computed analytically

$$n_j^{id} \approx n_j^B = g_j \, \left(\frac{T^3}{2\pi^2}\right) \left(\frac{m_j}{T}\right)^2 K_2\left(\frac{m_j}{T}\right) \, \exp\left(\frac{\mu_j}{T}\right) \equiv g_j \, \left(\frac{T^3}{2\pi^2}\right) W_j \, \exp\left(\frac{\mu_j}{T}\right), \tag{22}$$

and the strange chemical potential is obtained as [36]:

$$\mu_S = \frac{T}{2} \ln \frac{3\alpha W_s + v(1-\alpha)\left(W_K \, e^{-\frac{\mu_B}{3T}} + (W_\Lambda + 3W_\Sigma)e^{\frac{2\mu_B}{3T}}\right)}{3\alpha W_s + v(1-\alpha)\left(W_K \, e^{\frac{\mu_B}{3T}} + (W_\Lambda + 3W_\Sigma)e^{-\frac{2\mu_B}{3T}}\right)} + \frac{\mu_B}{3} \,. \tag{23}$$

It is seen that at the *plasma boundary* ($\alpha = 1$) $\mu_S = \mu_B/3$ while $\mu_S \neq \mu_B/3$ at the *hadron boundary* ($\alpha = 0$). This implies that not only μ_S but also μ_B and the pressure changes along isotherms in the coexistence region. Hence, the standard Maxwell construction, which interpolates the densities linearly between the pure phases, is not adequate. The equations for phase equilibrium (18–20) must be solved to obtain μ_S and μ_B at every point in the coexistence region.

When two phases coexist, the system is in general not homogeneous as the phases occupy a separate domains in space. We do not explicitly account for such domains structure nor for a possible surface energy contribution to the equation of state. The only consequence of the phase separation in this calculations is that the interactions between particles in the plasma and hadronic phase are excluded. This is different in the statistical mixed phase model discussed in the next section.

The solution of the Gibbs conditions (18–20) is shown in Fig. 1 for the plasma and hadron phase pressure versus μ_B^4 at fixed $T = 80$MeV and $\mu_S = \mu_B/3$. The crossing of the quark and hadronic pressure corresponds to the transition point at the plasma boundary. In this special case the condition $\mu_S = \mu_B/3$ guarantees strangeness neutrality. In general, however, for $\alpha \neq 1$, μ_S must be chosen such that the strangeness of the total system of quarks and hadrons vanishes. This requires an iterative solution of the equations (18–20). Away from the transition point, the system is in the phase with higher pressure p (lower free energy). Fig. 1 also shows that there is no deconfinement transition if the hadronic phase is described as a gas of point–like particles [34]. The situation is not improved by including more resonances. On the contrary, the larger the set of hadronic resonances is, the higher is the pressure at a given baryon chemical potential. However, the inclusion of repulsive interactions between hadrons leads to a reduction of the hadron pressure p^H at fixed baryon chemical potential. Consequently, a short–range repulsion between hadrons stabilizes the quark–gluon plasma at high densities.

The resulting phase boundaries in the T–μ plane are shown in Fig. 2. The difference in μ_B at the phase boundaries described by Eqs.(18–20) is small while for the strange chemical potential μ_S it is more noticeable. It is natural to expect that in the high temperature plasma $\mu_S \approx \mu_B/3$. On the other hand, in the hadronic phase and at low temperatures, where strangeness is carried mostly by kaons and Λ–hyperons, the strange chemical potential is roughly approximated by $\mu_S \approx 0.5 \left(\mu_B + m_K - m_\Lambda\right) \approx 550$MeV. Both these
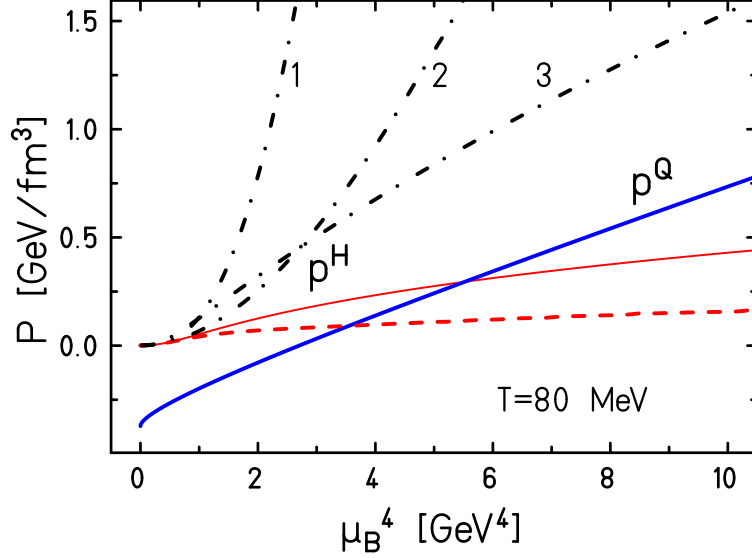
Figure 1: Pressure versus baryon chemical potential for fixed $T = 80\ MeV$ and for $\mu_S = \mu_B/3$. The thin–line is the hadronic and the thick–line the quark phase in 2PC model. The dashed–dotted (1) line and dashed–line are an ideal gas model results without and with repulsion in the 2PIN model, respectively. The line (2) is obtained as line (1) but with fewer hadronic resonances. The line (3) is calculated within a mean–field approximation of the Zimanyi model [37] (see text).

expectations are in agreement with our numerical results. Nevertheless, also in the high temperature hadronic phase the strange chemical potential exhibits an approximately linear dependence on the baryon chemical potential.

In Figs. 2 and 3, the resulting phase diagrams are shown in the T–μ_B and T–μ_S as well as T–n_B planes. The role of thermodynamical consistency is particularly evident in the T–n_B plane. As seen in Fig. 3, the baryon density n_B at the plasma boundary is increased while it is slightly decreased at the hadron side in the 2PC model as compared with the 2PIN approach. Consequently, the range of the coexistence region grows from $\sim (4 \div 7.5)n_0$
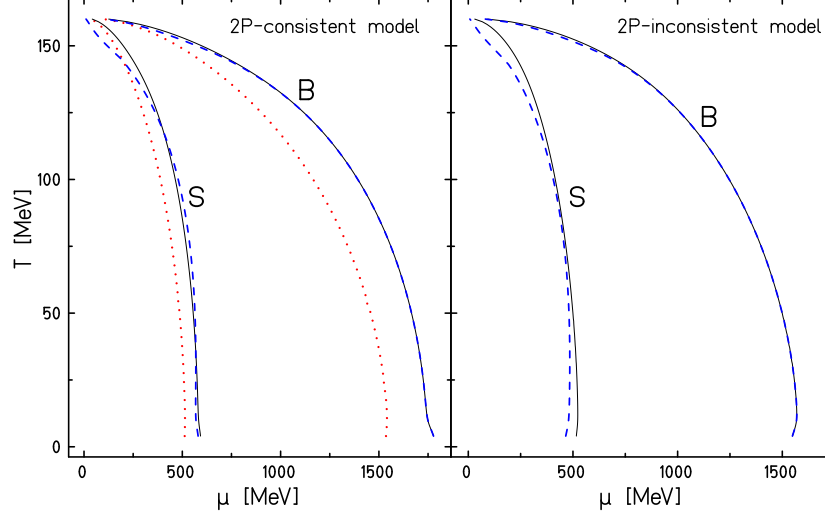
10

Figure 2: The phase diagram in the T–μ_B (marked by B) and in the T–μ_S (marked by S) plane for the 2PC and 2PIN models. The plasma and hadron boundaries are shown by full and dashed–lines, respectively. The dotted–lines are the approximate results obtained with $\mu_S = 0$ and with μ_S from Eq.(23).
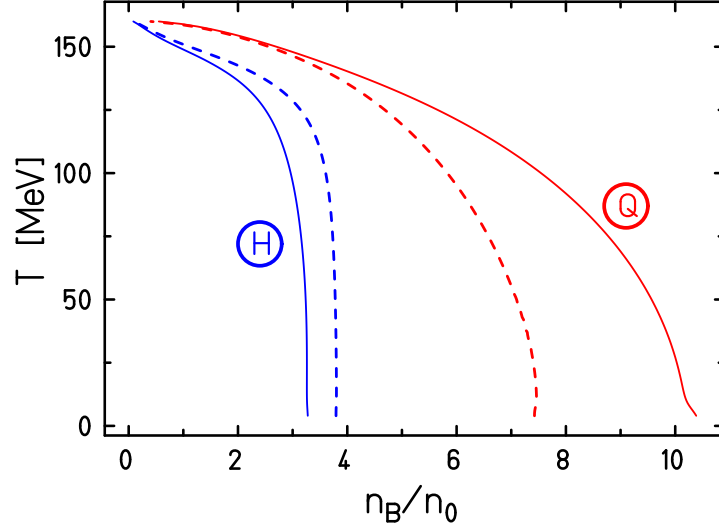

Figure 3: The phase diagram in the (T–n_B) plane for 2PC (full–lines) and 2PIN (dashed–lines) models.
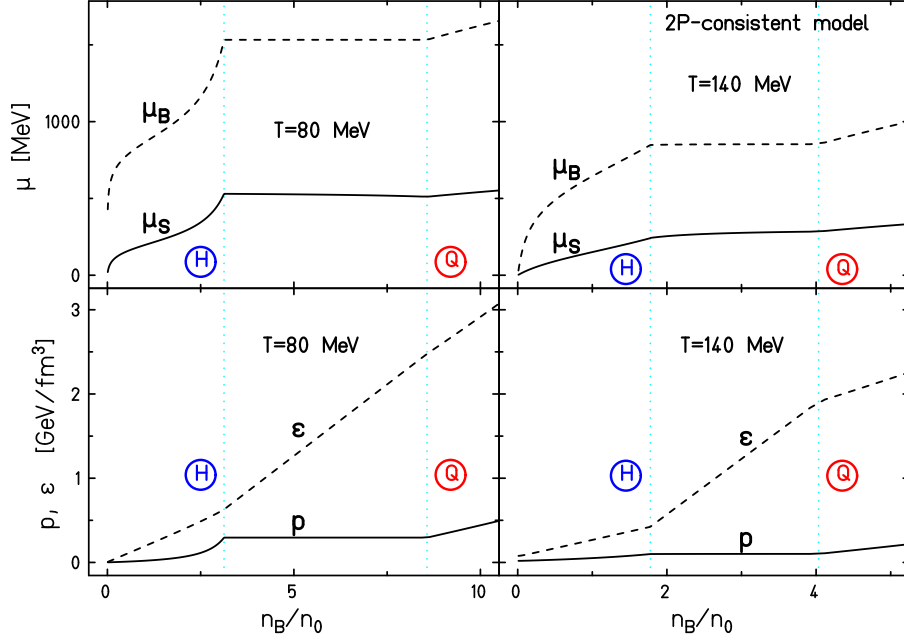
to $\sim (3.5 \div 10)n_0$.

Figure 4: Dependence of different thermodynamical quantities on the baryon density within 2PC model. The results are shown for two different temperatures. The hadron and plasma phase boundaries are shown by dotted–lines.

Thermodynamical properties and the differences between the two–phase bag models are shown in Figs. 4 and 5. In both cases the baryon and strange chemical potentials are continuous when crossing the phase boundaries. This guarantees that the system is chemically stable. Demanding the conservation of strangeness in each phase separately [20] would results in a discontinuity in μ_S . In contrast to the case with only one conserved charge, the chemical potentials are not necessary constant within the Gibbs coexistence region. Depending on the values of μ at the hadronic and plasma boundaries (see Fig. 2), the chemical potentials (in particular μ_S) can be either increasing or decreasing functions of n_B. Although this change is not large, it influences the strangeness separation in the phase coexistence region.

The energy density is seen in Figs. 4 and 5 to be a monotonously increasing function of n_B in both models. The pressure is also continuous

within 2PC model and is higher than in the 2PIN approach. In addition, in the latter model the pressure also suffers a jump at the boundary of the hadronic phase, which increases with decreasing temperature. Such an EoS would lead to a mechanical instability of the hydrodynamic flow. As seen in Figs. 4 and 5, the changes in pressure across the coexistence region are quite small. Consequently, the system expands very slowly. This is a specific feature expected for the systems with a first order phase transition.
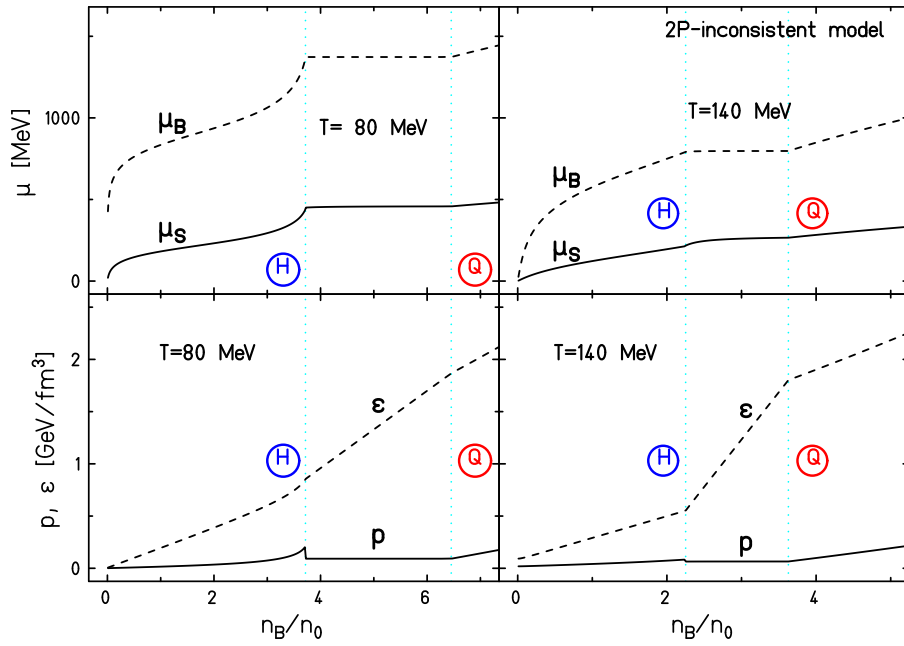

Figure 5: The same as in Fig. 4 but for the 2PIN model.

We stress that there are at least two problems, which show up when the EoS discussed above is employed in hydrodynamic calculations. First, as shown in [36, 38] causality is violated at densities $n_B \gtrsim 3.5 n_0$. Second, the ideal gas model with an excluded volume correction does not reproduce the saturation properties of nuclear matter. An attempt to combine the excluded volume correction with a mean field treatment of the hadronic interactions resulted in an incompressibility parameter which is too large $K \geq 550 \ MeV$ [36].

13

2.2 Statistical mixed phase model

The mixed phase (MP) model [28, 29, 39] is a phenomenological model of the EoS with a deconfinement phase transition of QCD which shows a satisfactory agreement with the lattice data. The underlying assumption of the MP model is that unbound quarks and gluons *may coexist* with hadrons forming a *spatially homogeneous* quark/gluon–hadron phase which we call a generalized Gibbs mixed phase. Since the mean distance between hadrons and quarks/gluons in the mixed phase may be of the same order as that between hadrons, the interactions between all these constituents (unbound quarks/gluons and hadrons) play an important role. The strength of this interactions defines the order of the phase transition.

To find the free energy within the MP model [28, 29], the following effective Hamiltonian, expressed in terms of quasiparticles interacting with a density–dependent mean field, is used :

$$H = \sum_i \sum_\sigma \int d\mathbf{r} \; \psi_i^+(\mathbf{r}, \sigma) \; \left(\sqrt{-\nabla^2 + m_i^2} + U_i(\rho) \right) \; \psi_i(\mathbf{r}, \sigma) - C(\rho)V \; . \tag{24}$$

Here $\psi_i(\mathbf{r}, \sigma)$ denotes a field operator for the quasiparticle species i characterized by the mass m_i (the current masses for quarks and gluons and the free hadron masses are used here). The index σ accounts for spin, isospin and color degrees of freedom. Furthermore, U_i is the mean field acting on particles of type i, $C(\rho)$ is a potential energy term, which is needed to avoid double counting of the interaction, and V is the volume of the system.

By requiring thermodynamical consistency [28, 29, 30, 31] one finds constraints on the parameters in the Hamiltonian. The constraints follow from [28, 29]

$$\langle \frac{\partial H}{\partial T} \rangle = 0 \,, \quad \langle \frac{\partial H}{\partial \rho_i} \rangle = 0 \;, \tag{25}$$

where $\langle \ldots \rangle$ denotes the statistical average. For the Hamiltonian (24), these conditions reduce to

$$\sum_i \rho_i \frac{\partial U_i}{\partial \rho_j} - \frac{\partial C}{\partial \rho_j} = 0 \;, \quad \sum_i \rho_i \frac{\partial U_i}{\partial T} - \frac{\partial C}{\partial T} = 0 \,, \tag{26}$$

which, as shown in [28, 29] , imply that $U_i(\rho)$ and $C(\rho)$ do not explicitly depend on temperature.

We model color confinement by assuming the following density dependence for the mean–field potential of quarks and gluons

$$U_q(\rho) = U_g(\rho) = \frac{A}{\rho^\gamma} \; ; \quad \gamma > 0 \tag{27}$$

where

$$\rho = \rho_q + \rho_g + \sum_j \rho_j = \rho_q + \rho_g + \sum_j \nu_j \, n_j \tag{28}$$

is the total number density of quarks and gluons in the local rest frame and ρ_q and ρ_g are the number densities of unbound (deconfined) quarks and gluons ($\rho_{pl} \equiv \rho_q + \rho_g$), while n_j is the number density of hadrons of type j having ν_j number of valence quarks inside. The presence of the total number density ρ in (27) implies interactions between all components of the generalized Gibbs mixed phase. The potential (27) exhibits two important limits of QCD. For $\rho \to 0$, the interaction potential approaches infinity, *i.e.* an infinite amount of energy is necessary to create an isolated quark or gluon. This obviously simulates confinement of colored objects. In the opposite limit of large energy density, $\rho \to \infty$, we have $U_g \to 0$ which is consistent with asymptotic freedom.

In the description of the hadron components, the MP model accounts not only for hadron–hadron but also for quark/gluon–hadron interactions. The mean field acting on the hadron species j in the MP model has two terms :

$$U_j = U_j^{(h)} + U_j^{(pl)} \; . \tag{29}$$

In the limit where there are no unbounded quarks and gluons, $U_j^{(pl)} = 0$, i.e., $U_j = U_j^{(h)}$. This happens at low densities, where colored degrees of freedom are confined in hadrons.

Due to the constraints (26) the second term in Eq.(29) my be written as [28]:

$$U_j^{(pl)} = \frac{\nu_j A}{\rho^\gamma} \left(1 - (1 - w_{pl})^{-\gamma}\right) \; , \tag{30}$$

where $w_{pl} = \rho_{pl}/\rho$ is the fraction of quark–gluon plasma in the mixed phase [1]. Thus, if U_q and U_g are known, the thermodynamic consistency conditions (26) allow us to unambiguously determine the correction term $C(\rho)$ in Eq. (24).

---

[1]We note that the resulting hadron single particle potential becomes very attractive near the plasma phase boundary, and even diverges in the plasma phase. We do not believe that this behaviour is physical. Nevertheless, we adopt this convenient prescription, since it does not have a noticeable effect on the thermodynamics nor on the hydrodynamic flow.

The hadronic potential $U_j^{(h)}$ is described by a non-linear mean-field model [37]

$$U_j^{(h)} = g_{r,j}\,\varphi_1(x) + g_{a,j}\,\varphi_2(y)\,, \tag{31}$$

where $g_{r,j} > 0$ and $g_{a,j} < 0$ are repulsive and attractive coupling constants, respectively.

Thermodynamic consistency implies that the functions $\varphi_1(x)$ and $\varphi_2(y)$ depend only on particle densities. In Ref. [37] these functions are chosen such that

$$b_1\varphi_1 = x, \quad -b_1(\varphi_2 + b_2\varphi_2^3) = y \tag{32}$$

where

$$x = \sum_{\nu_i} g_{r,i}\,\rho_{\nu_i}, \quad y = \sum_{\nu_i} g_{a,i}\,\rho_{\nu_i}\,.$$

and b_1 and b_2 are free parameters. In [37] considering a mixture of nucleons and Δ's the model parameters were fixed such that to reproduce the saturation properties of nuclear matter and the ratio of the Δ to nucleon coupling constants. We generalize this approach by including all hadrons in our model and assuming that the coupling constants scale with the number of constituent quarks :

$$U_j^{(h)} = \nu_j\left(\widetilde{\varphi}_1(\rho - \rho_{pl}) + \widetilde{\varphi}_2(\rho - \rho_{pl})\right)\,, \tag{33}$$

where $\widetilde{\varphi}_1$ and $\widetilde{\varphi}_2$ satisfy the equations

$$c_1\widetilde{\varphi}_1 = \rho - \rho_{pl}, \quad -c_2\widetilde{\varphi}_2 - c_3\widetilde{\varphi}_2^3 = \rho - \rho_{pl} \tag{34}$$

with $\rho - \rho_{pl} = \sum_{\nu_j} \nu_j\rho_j$. The parameters in Eq. (34) are given by [28]

$$c_1 = \frac{b_1}{(g_{r,j}/\nu_j)^2}, \quad c_2 = \frac{b_1}{(g_{a,j}/\nu_j)^2}, \quad c_3 = \frac{b_1 b_2}{(g_{a,j}/\nu_j)^4}$$

and are fixed by requiring that the properties of the ground state ($T = 0$, $n_B = n_0 \approx 0.17\ fm^{-3}$) of nuclear matter are reproduced: i.e. a binding energy per nucleon of $-16\ MeV$, incompressibility of $210\ MeV$ and vanishing pressure.

We also addressed to the extension of the Zimanyi model [37] as interacting hadron gas (InHG) model with no phase transition. The μ_B–dependence of the pressure in this model is illustrated in Fig. 1.

16

The thermodynamics in the MP model is obtained from the partition function in the standard way. The baryon and strange chemical potentials are fixed by the baryon number and strangeness conservation,

$$n_B(T,\mu) = \sum_{j\in q,h} b_j \, n_j(T,\mu_j) , \qquad (35)$$

$$n_S(T,\mu) = 0 = \sum_{j\in q,h} s_j \, n_j(T,\mu_j) , \qquad (36)$$

where the sum is taken over all quarks, gluons and hadrons. The same set of hadrons and resonances is used here as in the previous models.

As an example we quote an expression for particle number density,

$$n_j(T,\mu_j) = \frac{g_j}{2\pi^2} \int_0^\infty dk k^2 \left[\exp\left(\frac{\sqrt{k^2+m_j^2} - b_j\mu_B - s_j\mu_S + U_j}{T} \right) \pm 1 \right]^{-1} . \qquad (37)$$

In the energy density and pressure there are further terms, originating from the interactions. These terms, are obtained [28, 29] by solving the consistency conditions (26).

2.3   Thermodynamics in the mixed phase model

The parameters of the MP model are fixed [28, 29] by requiring that the lattice results for thermodynamical quantities in the pure gauge and two flavor QCD are reproduced. In this study the quark–gluon interaction parameters $\gamma = 0.62$ and $A^{1/(3\gamma+1)} = 250$ MeV were obtained. The same parameters are assumed to be valid also for the interactions with strange quarks.

In Fig. 6 we compare the thermodynamical properties of the MP and 2PC models. The energy density and pressure in the 2PC model shows the typical behavior for a system with a first order phase transition: an abrupt change in the energy density at $T = T_c$ and smooth change in the pressure. In the MP model on the other hand, both ε and p vary continuously with temperature. The transition temperature in the MP model, $T_c \approx 160$ MeV, is defined by the maximum of the heat capacity (see insert in Fig. 6).

In Fig. 7 the ratio p/ε is shown for different values of the total baryon number density in three models under consideration. A common feature of these models is that for finite baryon densities they all exhibit a clear threshold behavior. The threshold is shifted to higher ε with increasing n_B. However, in contrast to the ideal hadron gas, both the MP model and 2P
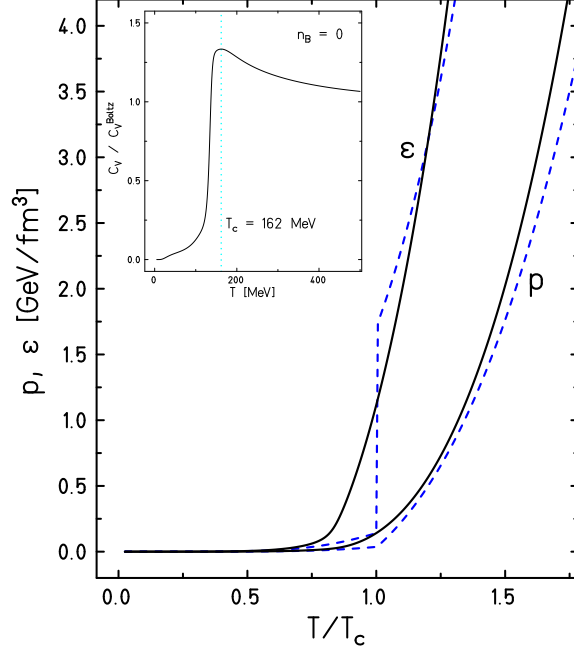
17

Figure 6: Temperature dependence of the energy density and pressure at vanishing total baryon density. Full and dashed–lines are the MP and 2PC model results, respectively. The insert figure shows the reduced heat capacity.

model have the *softest point* in the EoS, i.e., a minimum [26] of the function $p(\varepsilon)/\varepsilon$. A particular feature of the MP model is that even for $n_B = 0$ the softest point is not very pronounced and located at a relatively low energy density: $\varepsilon_{SP} \approx 0.45$ GeV/fm^3. This is consistent with lattice result [40]. In the MP model, the softest point is gradually washed out with increasing baryon density and vanishes completely for $n_B \gtrsim 0.5\ n_0$. This is, however, not the case in the 2P models, where one finds a pronounced softest point at large energy density $\varepsilon_{SP} \approx 1.5$ GeV/fm^3, which depends only weakly on the baryon density n_B see Fig. 7). Finally, in the InHG model as well as in the relativistic ideal hadron gas there is obviously no softest point in the EoS.

The differences in the thermodynamical properties of the above models will be also reflected in the expansion dynamics of a thermal fireball created in heavy ion collisions. The effect of these differences on strangeness production and evolution will be explored in the following sections.
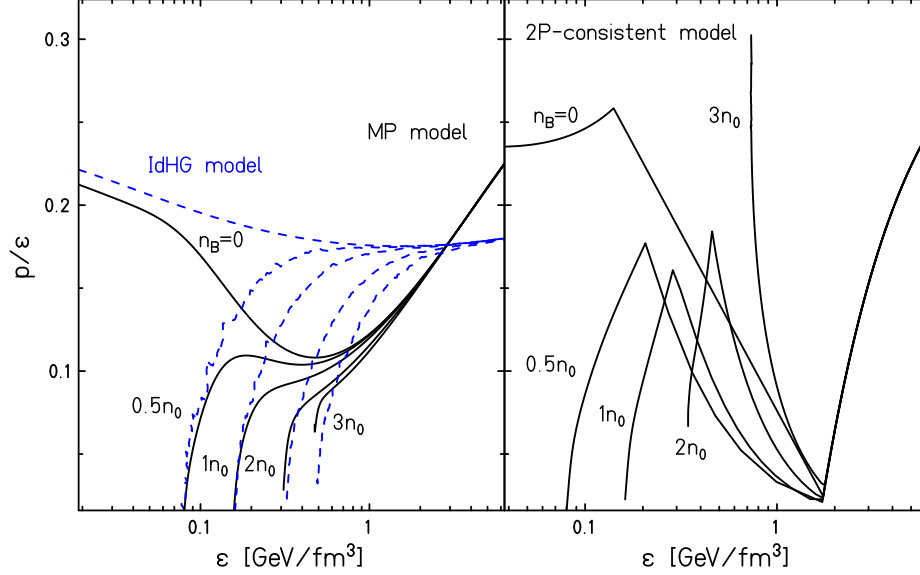
18

Figure 7: The ratio of the pressure (p) to the energy density (ϵ) as a function of ϵ. The results are for different values of a total baryon density (n_B) and for three models of the EoS.

3 Strangeness production

3.1 Strangeness content in equilibrium

The conservation of strangeness in the coexistence region of quarks and hadrons implies that the total number of strange and antistrange quarks are equal. However, the s–$\bar{s}$ content in the individual phases may differ from zero. The strangeness content of the quarks in the mixed or plasma phase is characterized by two ratios : $\rho_s/\rho_{\bar{s}}$ and $D_s = (\rho_s + \rho_{\bar{s}})/\rho_{pl}$ (see Eq. (28)). The second ratio gives the strangeness fraction in the plasma.

In Fig. 8 the ratio $\rho_s/\rho_{\bar{s}}$ is shown as a function of μ_B for a fixed plasma fraction α. For $\alpha \sim 1$ the ratio $\rho_s/\rho_{\bar{s}} \approx 1$ for almost all values of μ_B. However, if $\alpha << 1$, that is when the volume in the mixed phase is mostly occupied by hadrons, the separation of strange and antistrange quarks is clearly seen in Fig. 8. This is mainly because the hadronic component of the mixed phase is dominated by the kaons, while the hyperons are suppressed due to their large masses. This strangeness excess through kaons is compensated by creation of

19

s–quarks in the plasma. The results in Fig. 8 are in qualitative agreement with Ref. [22] where the 2PIN model without higher mass resonances was employed. The contribution of higher mass resonances results in an increase of $\rho_s/\rho_{\bar{s}}$ for $(\mu_B/3)_H \approx 400 - 500 \ MeV$.
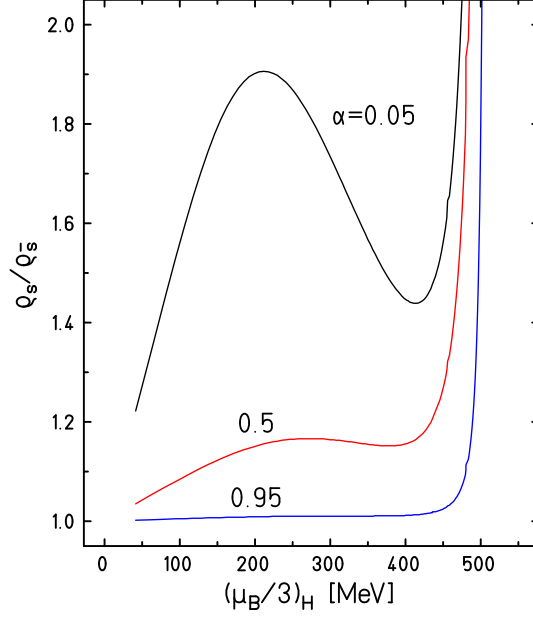

Figure 8: Ratio of strange to antistrange quark densities in a quark–gluon plasma calculated along the hadronic boundary. The results are for PC model calculated with different values of the volume fraction (α) occupied by a quark–gluon plasma.

In Fig. 9 the strangeness composition in an equilibrium system is compared for two different models. In the bag model EoS and at high temperature $(T \sim 140 \ MeV)$ the $\rho_s/\rho_{\bar{s}}$ ratio decreases when the baryon density inside the Gibbs mixed phase approaches the plasma boundary. However, for the moderate temperatures $(T \sim 80 \ MeV)$, the ratio $\rho_s/\rho_{\bar{s}} < 1$ and it increases with n_B. The above behavior is a direct implication of the simultaneous conservation of strangeness and the baryon number. If these conservation laws are decoupled [22], then this behavior at low temperatures is not seen.

In the MP model the $\rho_s/\rho_{\bar{s}} > 1$ for all values of the baryon density. For a fixed temperature the $\rho_s/\rho_{\bar{s}}$ ratio is seen in Fig. 9 to gradually decrease with
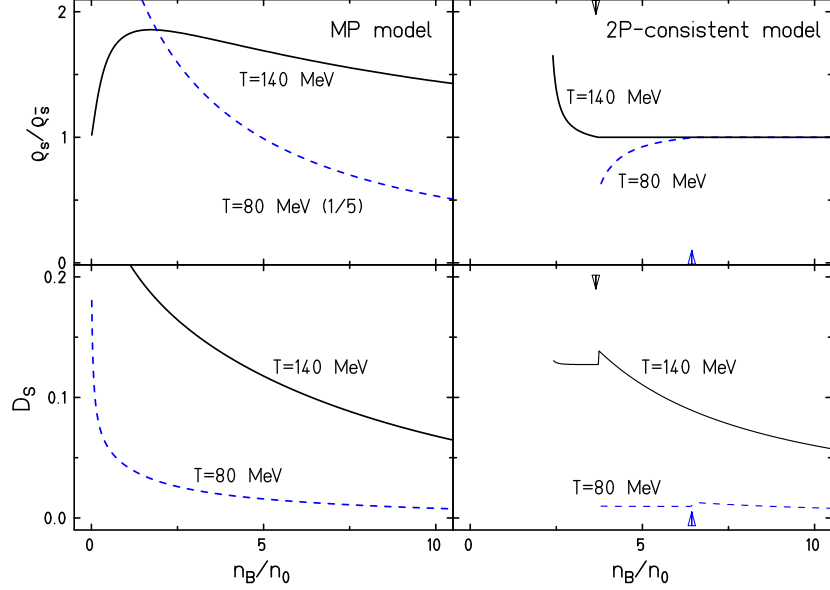
Figure 9: The $\rho_s/\rho_{\bar{s}}$ ratio for quark component and strangeness fraction (D_s) for unbound quarks as a function of baryon density. The results are shown for different temperatures and for two EoS. The plasma boundary is marked by arrows. Note the factor $1/5$ in the MP model at $T = 80$ MeV.

increasing density. Its values are noticeably higher than in the 2P model. In both models, however, the strangeness separation effect is stronger when the system is closer to the hadronic boundary, i.e. where there is small admixture of quarks. For the 2P model this corresponds to the existence of a small blob of plasma while in the MP model a homogeneous admixture of unbound quarks and gluons with small concentration.

Above the hadronic phase boundary, the n_B–dependence of D_s in the 2PC model is similar to that in the MP model. The strangeness fraction in the MP model is the largest below the hadronic boundary and maximal in baryon free matter. In Fig. 9 we note a jump in D_S which corresponds to a jump in strange particle multiplicity when crossing the phase boundary; a similar jump is observed in the baryon number.

From the above discussion, it is clear, that the strangeness content and its distribution in the transition region from the quark–gluon plasma to the

hadronic phase is strongly model dependent. It is effected by the order of the phase transition and the strength and the form of the interactions between constituents. These differences are particularly evident at moderate values of the temperature and baryon density. This is just the region which is traversed by an expanding system created in heavy ion collisions on its way towards the chemical freeze–out. Thus, one could expect that the order of the phase transition and particular strangeness dynamics could manifest itself in observables in heavy ion collisions.

3.2   Strangeness evolution in expansion dynamics

To study the possible influence of the EoS on observables in heavy ion collisions, we have to describe the space–time evolution of a thermal medium that is created in the initial state. This is conveniently done within a hydrodynamical model. The EoS is an input for constructing the energy—momentum tensor, which is needed in the hydrodynamical equations.

To solve the hydrodynamical equations for a given experimental set–up one needs to specify the initial conditions. The initial volume, the entropy and the baryon number densities in the collisions are modelled within QGSM transport code [41]. The predictions of this model are consistent with the results obtained within the RQMD and UrQMD transport codes.

We assume that, in the center of mass frame, the initial state is a cylinder of radius $R = 5\ fm$ and Lorentz contracted length $L = 2R/\gamma_{c.m.}$. This initial state corresponds to the time when the centers of the colliding nuclei just have passed the point of full overlap.[2] We neglect the transverse expansion and assume that the hydrodynamical evolution of the fireball is described by a one-dimensional isentropic expansion of the scaling type in the longitudinal direction. In this approximation the entropy and baryon density decrease inversely proportional to the expansion time. The values of all other thermodynamic quantities are obtained from the EoS at each temporal step (see, for example [42]).

In Fig. 10 we show the fireball evolution trajectories for central Au–Au collisions in the T–μ_B plane for different collision energies and for different EoS. The chemical freeze–out parameters obtained [8, 9, 43, 44] within the statistical model at different collision energies are also shown in this figure.

---

[2]A detailed description of the procedure to fix the initial conditions in heavy ion collisions can be found in [28, 29, 30, 31].

Clearly, the chemical freeze–out parameters from SIS up to RHIC are well described by the universal condition of fixed energy/particle, $\langle E_{had} \rangle / \langle N_{had} \rangle \simeq 1$ GeV [43, 45].
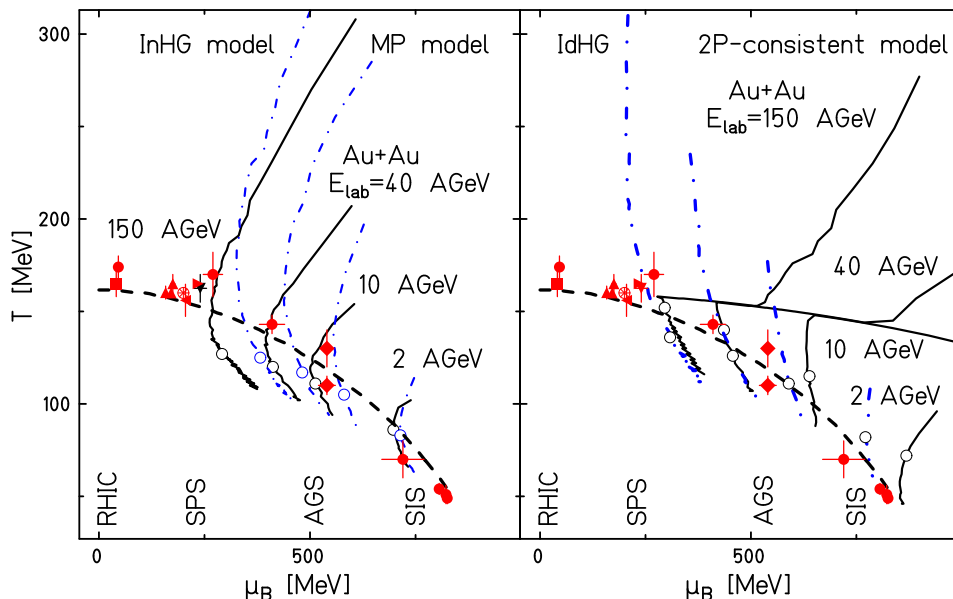

Figure 10: A compilation of the chemical freeze–out parameters from Refs. [9, 43, 44] obtained with the hadron resonance gas partition function at different beam–energies (filled dots, squares and triangles). The smooth dashed curve is the universal freeze–out curve of fixed $\langle E_{had} \rangle / \langle N_{had} \rangle \simeq 1 \; GeV$ from Ref. [43]. Also shown are dynamical trajectories for central Au–Au collisions calculated within different models (the interacting hadron gas model (InHG), the mixed-phase model (MP), the ideal hadron gas model (IdHG) and the thermodynamically consistent two–phase model (2PC)). The empty circles near the end of each trajectory correspond to freeze–out condition of fixed energy density, $\varepsilon_f \simeq 0.135 \; GeV/fm^3$.

The dynamical trajectories show a strong dependence on the properties of the EoS. In the MP model there is a turning point seen in all trajectories, i.e. the point where $\partial T / \partial \mu_B$ changes sign. The existence of such a point is a general feature of the MP model and is directly related to the appearance of two limiting regimes:

(i) At high temperatures and in the ultra–relativistic limit, $m_q \rightarrow 0$,

the thermodynamic potential $\Omega = -Vp$ can be obtained analytically from Eqs.(9) and (12)

$$\Omega = -V \left(a_1 T^4 + a_2 T^2 \mu_B^2 + a_3 \mu_B^4\right) . \tag{38}$$

The entropy per baryon

$$\frac{s}{n_B} = \frac{\partial\Omega/\partial T}{\partial\Omega/\partial\mu_B} = \frac{2a_1 + a_2 \left(\frac{\mu_B}{T}\right)^2}{a_2 \left(\frac{\mu_B}{T}\right) + a_3 \left(\frac{\mu_B}{T}\right)^3} , \tag{39}$$

is conserved along trajectories defined by $\mu_B/T = const$. Thus, in the high temperature limit, an isentropic expansion is characterized by a linear relation between T and μ_B.

(ii) At intermediate temperatures, the system can be approximated by a Boltzmann gas (22) of a non–relativistic nucleons. In this case the entropy in the dilute gas approximation is given by

$$
\begin{aligned}
S &= -\frac{g_N V}{(2\pi)^3} \int d^3p \; [f \ln f + (1 - f) \ln(1 - f)] \\
&\approx N_B \left[1 - \frac{\int d^3p \; f \ln f}{\int d^3p \; f}\right]
\end{aligned}
\tag{40}
$$

with the distribution function $f = \exp[(\mu_B - m_B - p^2/2m_B)/T]$. In this temperature range, conservation of the entropy per baryon implies that

$$\frac{s}{n_B} = \frac{5}{2} + \frac{m_B - \mu_B}{T} = const . \tag{41}$$

Thus, for intermediate temperatures, we again find a linear relation between T and μ_B but with a negative slope. The different behavior of $\mu_B(T)$ at high and intermediate temperatures, implies that there is a turning point in the fireball expansion trajectories, as seen in Fig. 10.

The dynamical trajectories calculated in the MP model pass quite close to the phenomenological freeze–out points. For all collision energies, the turning point is located on the universal freeze–out curve of fixed energy/particle. This fact has been noticed already in Ref. [46] for the MP model with two light quarks. The contribution of strange quarks and the requirement of strangeness conservation modifies the dynamical expansion path of the fireball. This is particularly evident for $E_{lab} \lesssim 10$ AGeV where neglecting

24

the strange quarks gives rise to a visible shift of the turning point towards smaller μ_B.

In the parameter range below the phenomenological freeze–out curve the expansion path in the MP, IdHG as well as in MP model are quite similar. In the InHG model, however, there is a small shift toward larger values of μ_B. This agreement indicates that in the final stage the expansion path depends only weakly on details of the equation of state. The dynamical path is, to a large extent, determined by the entropy/baryon and strangeness conservation which in the hadronic phase puts strong constraints on the particle composition of the fireball. In this case the space time evolution and thermodynamics is governed by a gas of weakly interacting resonances, the effective degrees of freedom in the low temperature phase of QCD. This may be the reason behind the success of the non–interacting hadron resonance gas in the description of bulk observables in heavy ion collisions.

The differences between the various equations of state in the evolution of the thermal fireball is clearly visible above the freeze–out curve. In contrast to the MP model, the IdHG turning points do not correlate with the freeze–out curve. There is also no softest point in the InHG and IdHG model. The dynamical trajectories within the 2P bag–models exhibit a characteristic re–heating regime in the phase coexistence region. For this model, the expansion trajectory closely follows the phase boundary in this regime, as shown in Fig. 2. At SPS energies and above, the hadronic end of the intermediate coexistence region in the T–μ_B plane (the so–called "hottest hadronic point") is close to the phenomenological chemical freeze–out point. At lower energies there is no such correlation for the 2P models. For $E_{lab} \lesssim 10 \ AGeV$ the initial state is in the phase coexistence region.

The question of strangeness separation in heavy ion collisions addressed in Ref. [22] for static system can be reanalyzed in our approach for dynamically evolving fireball. The results are shown in Fig. 11 for Au–Au collisions at different bombarding energies within 2P and MP models. In both models $\rho_s/\rho_{\bar{s}} > 1$, since there is no chance for the system to pass through a high density baryonic state where ρ_s could be less then unity.

In the 2P model we find that strangeness is separated to a less degree at the exit point from the phase coexistence region than found in [22]. On the other hand in the MP model the system evolves much longer and consequently a higher degree of strangeness separation is obtained. This effect is stronger at $E_{lab} = 10 \ AGeV$ than at $160 \ AGeV$.

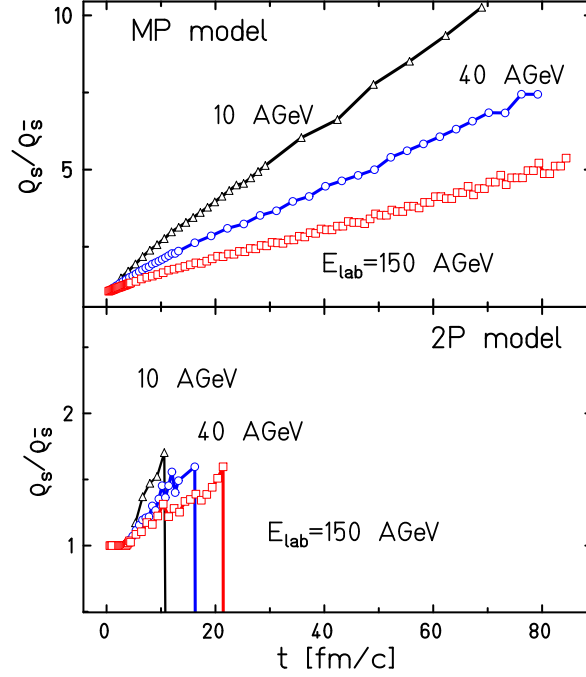So far the differences between various models for the expansion dynamics

Figure 11: Time evolution of the ratio of strange to anti–strange quark densities in the hadronic component. The MP and 2P model results are for central Au–Au collisions at different beam–energies.

were discussed on the level of global thermodynamical quantities. It is of particular interest to explore physical observables that are directly measured in heavy ion collisions. In the following we consider strange particle multiplicity ratios to discuss the influence of the equation of state on particle yields. The predictions of the different models will be compared at *thermal freeze–out* where the particle momentum distributions are frozen. We assume a shock–like freeze–out [47] where energy, the total baryonic and strangeness charges are conserved. The thermal freeze–out conditions are assumed to be determined by the fixed energy density $\varepsilon_f \approx 0.9 n_0 m_N = 0.135 \ GeV/fm^3$. Below this energy density the system consists of a free streaming gas of non interacting particles. The thermal freeze–out points are shown in Fig. 10 by empty circles on each trajectory for all models and for all collision energies.

The excitation function of the relative yields of K^+ mesons calculated within the MP model is shown in Fig. 12 as triangles. For reference, we also

show in this figure the 4π–integrated data for K^+/π^+ ratio obtained in heavy ion collisions at different beam energies. The shape of the kaon excitation function in the MP model is similar to that seen in the data. However, the absolute values are overestimated, especially for the low collision energies. We have to stress, however, that the models discussed here are still not quite suitable to be compared with data. First, the conservation of electric charge was not taken into account. The isospin asymmetry is particularly relevant at low collision energies (below AGS) where it can change the charge particle multiplicity ratios by up to 20%. Second, the hydrodynamical model applied here describes a longitudinally expanding fireball. This is, to a large extend sufficient at RHIC energies, however, it may be not valid at AGS or SIS where transverse expansion cannot be neglected. Furthermore, only part of particle mass spectrum was included with the masses up to 1.6 GeV. At AGS and higher energies the contributions from heavier resonances increases the yields of lighter particles. Finally, the system may be out of chemical equilibrium at some stages during the evolution from chemical towards thermal equilibrium [48]. Nevertheless, all these effects cannot account for the observed discrepancy by a factor of five between the MP model and data at low collision energies (Fig. 12). However, the differences may be due to the grand canonical (GC) treatment of the strangeness conservation used in the calculations.

In the GC ensemble strangeness is conserved on the average and is controlled by the strange chemical potential. Within the statistical approach, the use of the grand canonical ensemble for particle production can be justified only if the number of produced particles that carry a conserved charge is sufficiently large. In this case also event–averaged multiplicities can be treated in a grand canonical formulation. In this approach, the net value of a given charge (e.g. electric charge, baryon number, strangeness, charm, etc.) fluctuates from event to event. These fluctuations can be neglected (relative to the mean particle multiplicity) only if the particles carrying the charges in question are abundant. Here, the charge is indeed conserved on the average and a grand canonical treatment is adequate. However, in the opposite limit of low production yields (as is the case for strangeness production in low energy heavy-ion collisions) the particle number fluctuation can be of the same order as the event averaged value. In this case charge conservation has to be implemented exactly in each event [8, 49]. In the statistical physics the exact conservation of quantum numbers requires a canonical (C) formulation of the partition function.
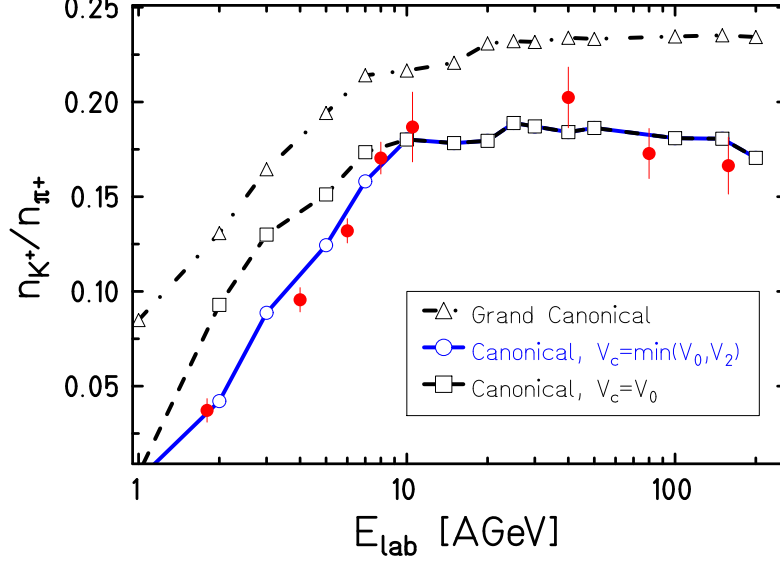
Figure 12: The K^+/π^+ ratio as a function of a beam–energy. The data points are from [44]. The lines are the MP model results obtained in the grand canonical as well as canonical formulation of strangeness conservation for different parameterizations of the volume parameter V_c (see text).

The grand canonical Z^{GC} and canonical Z_S^C partition functions are connected by a cluster decomposition in the fugacity parameter $(\lambda \equiv \exp(\mu_s/T))$

$$Z^{GC}(T,V,\mu_B,\lambda) = \sum_{s=-\infty}^{s=\infty} \lambda^s \; Z_s^C(T,V,\mu_B) \; . \qquad (42)$$

The relation (42) can be inverted and the canonical partition function with total strangeness $S = 0$ is obtained from

$$Z_{S=0}^C(T,V,\mu_B) = \frac{1}{2\pi} \int_0^{2\pi} d\phi \; Z^{GC}(T,V,\mu_B,\lambda \to e^{i\phi}) \; . \qquad (43)$$

Neglecting the contributions from multistrange hyperons and assuming Boltzmann statistics the density of kaons in the C ensemble is given by [50, 51]

$$n_K^C = n_K^B \; \frac{\mathcal{S}_1}{\sqrt{\mathcal{S}_1 \mathcal{S}_{-1}}} \; \frac{I_1(x)}{I_0(x)} \; . \qquad (44)$$

28

where the argument of the Bessel function $I_s(x)$ is

$$x \equiv 2\sqrt{\mathcal{S}_1 \mathcal{S}_{-1}}. \tag{45}$$

with

$$\mathcal{S}_s = V_c \sum_j n_j^B \ .$$

Here the particle density n_j^B for hadron species j is given by Eq. (22) with $\mu_j = \mu_B b_j$. The sum is taken over all particles and resonances carrying strangeness s. The volume V_c is a model parameter which is interpreted as the strangeness correlation volume.[3] In the equilibrium statistical model a correlation volume $V \equiv V_1 \simeq 1.9\pi A_{part}/2$ was found to reproduce the experimental multiplicity ratios for all measured particle. In our dynamical approach, V_c is assumed to be the initial volume of the collision fireball $V_c = V_0(E_{lab})$, and thus is energy dependent [52].

From Eqs.(44) and (22) it is clear that grand canonical and canonical results for the kaon density are related by the substitution [7]:

$$\exp(\mu_s/T) \to \frac{\mathcal{S}_1}{\sqrt{\mathcal{S}_1 \mathcal{S}_{-1}}} \frac{I_1(x)}{I_0(x)} \ . \tag{46}$$

Thus, the main difference between C and GC results is contained in a reduction of the fugacity parameter by the factor $F \equiv I_1(x)/I_0(x)$. In the limit of a large volume V_c, i.e., $x \to \infty$, the ratio $F \to 1$ and the GC and C results coincide. However, in the opposite limit, $x \to 0$, the factor $F < 1$ which leads to a suppression of the strange particle densities. The canonical suppression depends strongly on the temperature and the correlation volume. Both these parameters, in particular the temperature, are dependent on the collision energy.

The sensitivity of the suppression factor on E_{lab} and the correlation volume is shown in Fig. 13. The canonical suppression factor calculated with $V_c = V_1$ is increasing with collision energy and reaches its asymptotic value at $E_{lab} > 10$ GeV. Obviously the magnitude of the suppression is strongly dependent on the correlation volume. This is shown in Fig. 13 for three different parameterizations of V_c. Particularly interesting is the behavior of F for $V_c = V_0(E_{lab})$. Due to the Lorentz contraction the initial volume is

---

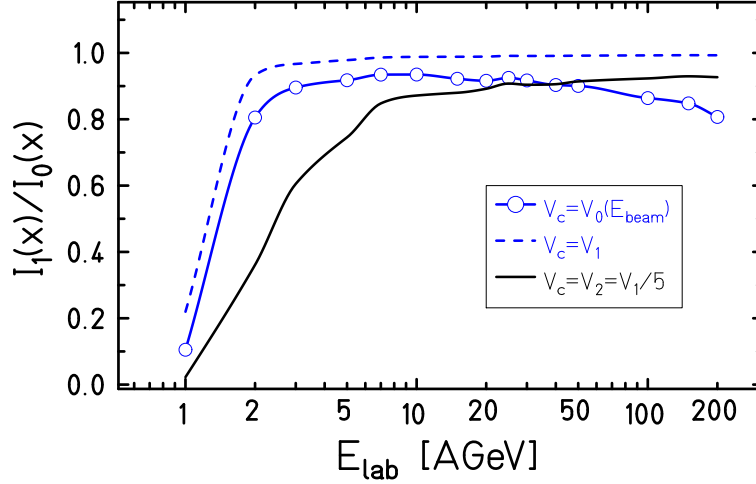[3]For a more detailed discussion of the interpretation and the role of this parameter see e.g. Ref. [8].

Figure 13: The beam–energy dependence of the strangeness suppression factor for central Au–Au collisions. This factor is calculated within MP model at freeze–out for different parameterizations of the correlation volume V_c (see text).

decreasing with increasing collision energy. At lower collision energies this decrease of the volume is compensated by an increase of temperature such that the suppression factor increases with E_{lab}. However for $E_{lab} > 10$ GeV there is only a moderate increase of freeze–out temperature that is not sufficient to overcome a decrease of V_0. Consequently for $E_{lab} > 10$ GeV the suppression factor starts to decrease with energy.

The amount of canonical suppression at fixed E_{lab} also depends strongly on the temperature which in turn is determined by the energy density at freeze–out. In the equilibrium analysis of particle production at SIS [7] the energy density at chemical and thermal freeze–out was a factor of three lower than the value used in the present dynamical study, $\epsilon \simeq 0.135$ GeV/fm^3. Consequently, for $V_c = V_0$ and for $1 < E_{lab} < 2$ GeV the canonical suppression found in Ref. [7] was much stronger than that shown in Fig. 13. We have not tuned the parameters to reproduce previous results. In low energy heavy ion collisions the expansion trajectories and the freeze–out parameters will change once the transverse expansion is taken into account.

In fig. 12 we show the effect of the canonical suppression on the K^+

excitation function calculated in the MP model with two different parame-terizations of the correlation volume: $V_c = V_0$ and $V_c = \min(V_0, V_2)$ where $V_2 = V_1/5$. As expected, there is a noticeable decrease of K^+ yield due to the exact treatment of strangeness conservation. The suppression of strangeness at energies beyond AGS is entirely due to the energy–dependent Lorentz contraction of the initial correlation volume. In Fig. 12 the results of a cal-culation also are presented where the choice of $V_c = \min(V_0, V_2)$ is optimized to reproduce the K^+/π^+ data.
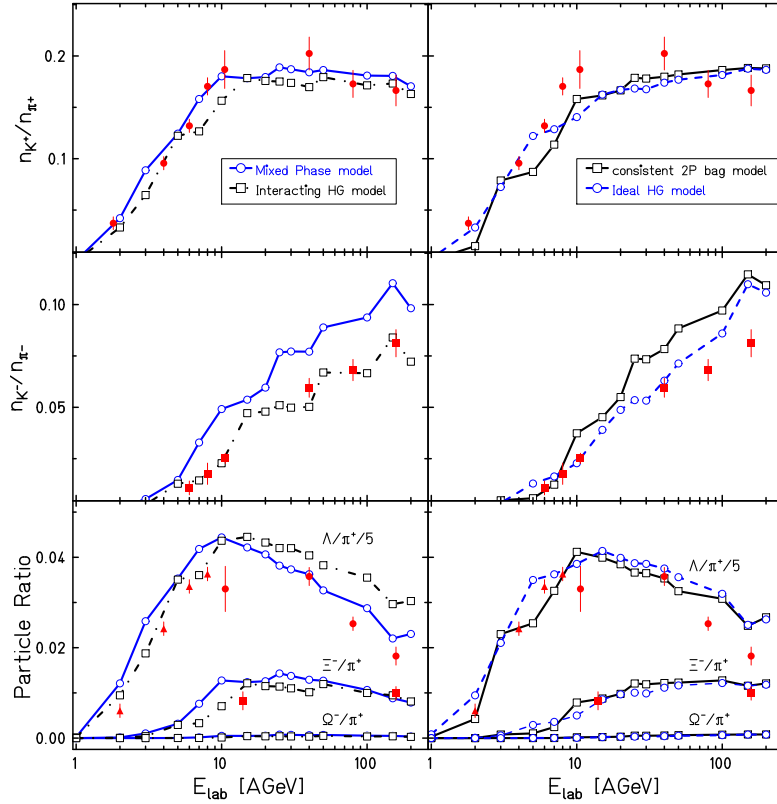

Figure 14: The ratios of 4π–integrated strange particle yields per pion yields for central Au–Au collision as a function of beam–energy. The compilation of experimental data is taken from [44, 53]. The calculated excitation functions are for different EoS with the canonical suppression factor.

The above analysis of K^+ excitation function clearly shows that due to

associated strangeness production and the small production cross sections at low collision energies one has to implement exact strangeness conservation. In the following we will implement this concept in all models and discuss the predictions for strangeness production and energy dependence. In the calculations we use the correlation volume $V_c = \min(V_0, V_2)$.

In Fig. 14 we calculate relative excitation functions for different strange mesons and baryons for four hydrodynamical models. The most striking result seen in this figure is that all models yield very similar results for the strangeness excitation functions. This is particularly true for the production of K^+/π^+ and Λ/π^+ where the results of all models besides InHG, are hardly distinguishable. Some differences are seen on the level of K^- excitation function which are mainly due to larger sensitivity of K^-/π^- ratio to the value of the temperature. It is interesting to note that all models show a maximum in the Λ/π excitation function for $10 < E_{lab} < 30$ GeV. Such a maximum is found also in equilibrium models [54].
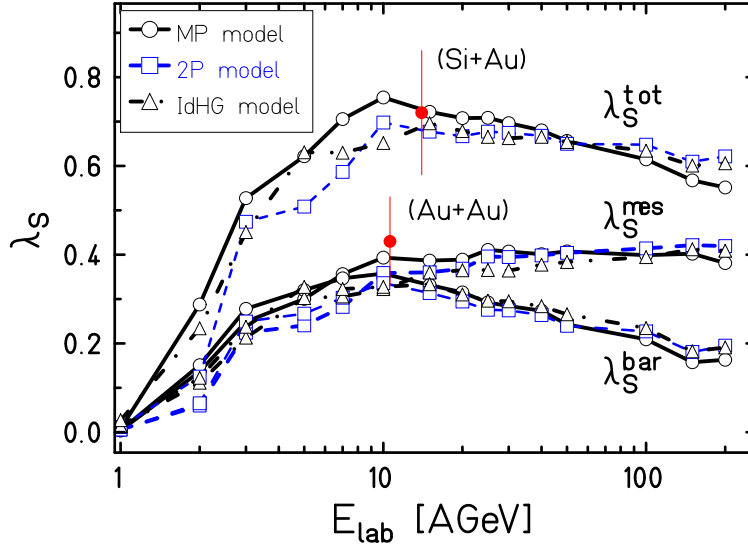

Figure 15: The Wroblewski ratio λ_s as a function of beam–energy for central Au–Au collisions. The contributions of mesons and baryons are shown separately. The points at AGS energies are from [44].

The relative strangeness content of the produced particles in heavy ion collisions is characterized by the Wròblewski factor [54, 55],

$$\lambda_S = \frac{2 < s\bar{s} >}{< u\bar{u} > + < d\bar{d} >} \tag{47}$$

where the quantities in angular brackets refer to the number of newly created quark–antiquark *pairs*. The Wroblewski factor is shown in Fig. 15 for different collision energies. The separate contributions to λ_S from strange mesons and baryons as well as its overall value is calculated within the MP, 2P and IdHG models. The results are compared with λ_S obtained in an equilibrium model analysis of experimental data at AGS energies. There is a surprising agreement of all dynamical models on the relative strangeness content of the fireball at freeze–out. The results are also consistent with the equilibrium model [54]. However, the maximum spread of the Wroblewski factor seen in Fig. 15 is broader than previously seen in the equilibrium canonical model [54]. In the dynamical models there is also a small shift in the position of this maximum towards lower energy.

4 Summary and conclusions

The main objective of this article was to explore the influence of the expansion dynamics, the equation of state and the nature of deconfinement phase transition on strangeness production in heavy ion collisions.

We have discussed and formulated different models for a phase transition in hight density QCD matter. The thermodynamical properties of these models and the role of the order of the phase transition as well as the interactions between the particles has been analyzed. We have addressed the question of the Gibbs construction of the phase transition in the presence of two conserved charges and emphasized the problem of causality and thermodynamical consistency.

The strangeness separation in the transition region from the quark–gluon plasma to the hadronic phase was also studied. The asymmetry in the relative concentration of strange and anti–strange quarks in the hadronic and quark–gluon component in the phase coexistence region was found in all models that exhibit a phase transition. However, the largest effect was observed in the mixed–phase model with a crossover–type deconfinement phase transition.

The differences in equilibrium thermodynamics of the models were studied on the dynamical level. We have shown that the hydrodynamical expansion trajectories of the fireball in the T–μ_B plane are very sensitive to the

equation of state. We considered the effect of the different expansion paths on strangeness production. Our detailed analysis show that there is almost no sensitivity of strangeness observables on the equation of state or on the expansion trajectories. This was demonstrated for several strange particle excitation functions.

To relate the model predictions with experimental data we have extended our study to a canonical formulation of strangeness conservation. We have discussed the phenomenological limitations of our dynamical models and the possible extension needed to provide a quantitative description of the observed particle yields in heavy ion collisions.

Exact strangeness conservation substantially reduces the strange particle yields in heavy ion collisions for $E_{lab} < 10$ GeV. For higher energies a moderate suppression is also found if the beam–energy dependence of the volume parameter V_c is taken into account. We have shown that the assumption that V_c is the volume of the initially produced Lorentz contracted fireball may lead to a negative slope in the energy dependence of the K^+/π^+ ratio. However, within considered models, the almost singular behavior of the excitation function near $E_{lab} < 20$ GeV for K^+/π^+ ratio found recently by the NA49 collaboration [56] was not reproduced. Simplified hydrodynamics with the assumption of a shock–like particles freeze–out in heavy-ion collisions results in a very smooth behavior of the strange particle excitation functions.

Acknowledgements

References

[1] For a review see eg. H. Satz, *Rep. Prog. Phys.* **63**, 1511 (2000); S.A. Bass, M. Gyulassy, H. Stöcker, and W. Greiner, *J. Phys.* **G25**, R1 (1999); E.V. Shuryak, *Phys. Rep.* **115**, 151 (1984).

[2] F. Karsch, E. Laermann, and A. Peikert, *Nucl. Phys.* **B605**, 579 (2001).

[3] See e.g., U. Heinz and S.M.H. Wong, *Nucl. Phys.* **A715** 649 (1993); I. Vitev and M. Gyulassy, *Phys. Rev. Lett.* **89** 252301 (2002); X.-N. Wang, nucl-th/0307036; E.L. Bratkovskaya, et al., nucl-th/0307098.

[4] See eg. Proceedings of Quark Matter 2002, *Nucl. Phys.* **A715**, (2002).

[5] J. Rafelski, *Phys. Rep.* **88**, 331 (1982); P. Koch, B. Müller and J. Rafelski, *Phys. Rep.* **142**, 167 (1986).

[6] P. Braun-Munzinger, I. Heppe and J. Stachel, *Phys. Lett.* **B465**, 15 (1999).

[7] J. Cleymans, H. Oeschler and K. Redlich, *Phys. Rev.* **C59**, 1663 (1999); *Phys. Lett.* **B485**, 27 (2000); H. Oeschler, *J. Phys.* **G27**, 257 (2001).

[8] P. Braun-Munzinger, K. Redlich and J. Stachel, nucl-th/0304013.

[9] F. Becattini, et al., *Phys. Rev.* **C64**, 024901 (2001); K. Redlich, *Nucl. Phys.* **A698**, 94c (2002); P. Braun-Munzinger, D. Magestro, K. Redlich and J. Stachel, *Phys. Lett.* **B518**, 41 (2001); W. Broniowski and W. Florkowski, *Phys. Rev.* **C65**, 064905 (2002).

[10] R. Averbeck, R. Holzmann, V. Metag and R.S. Simon, *Phys. Rev.* **C67**, 024903 (2003).

[11] W. Cassing, *Nucl. Phys.* **A661**, 468c (1999).

[12] J.C. Dunlop and A. Ogilve, *Phys. Rev.* **C61**, 031901 (1999); A. Ogilve, nucl-ex/0104010.

[13] F. Karsch, *Lect. Notes. Phys.* **583**, 202 (2002); E. Laermann and O. Philipsen, hep-ph/0303042.

[14] Z. Fodor, S.D. Katz and K.K. Szabó, hep-lat/0208078; C.R. All-ton, S. Ejiri, S.J. Hands, O. Kaczmarek, F. Karsch, E. Laermann and C. Schmidt, hep-lat/0305007, to appear in *Phys. Rev.* **D**, (2003); Z. Fodor, S.D. Katz and K.K. Szabó, hep-lat/0208078.

[15] F. Karsch, K. Redlich and A. Tawfik, hep-ph/0303108, to appear in *Eur. Phys. J.* (2003).

[16] F. Karsch, K. Redlich and A. Tawfik, hep-ph/0306208, to appear in *Phys. Lett.* **B** (2003).

[17] J.P. Blaizot, E. Iancu, and A. Rebhan, *Phys. Rev.* **D63**, 065003 (2001).

[18] A. Peshier, B. Kämpfer and G. Soff, *Phys. Rev.* **C61**, 045203 (2000); *Phys. Rev.* **D66**, 094003 (2002); J. Letessier and J. Rafelski, *Phys. Rev.* **C67**, 031902 (2003); K.K. Szabo and A.I. Toth, *JHEP* **306**, 008 (2003).

[19] A. Dumitru and R.D. Pisarski, *Phys. Lett.* **B525** 95 (2002); A. Dumitru and R.D. Pisarski, *Phys. Rev.* **D66** 096003 (2002); hep-ph/0204223.

[20] K.S. Lee, M.J. Rhoades-Brown and U. Heinz, *Phys. Lett.* **B174**, 123 (1986).

[21] B. Lucász, J. Zimányi and N.L. Balazs, *Phys. Lett.* **B183**, 27 (1987).

[22] C. Greiner, P. Koch and H. Stöcker, *Phys. Rev. Lett.* **58**, 1825 (1987).

[23] H.W. Barz, B.L. Friman, J. Knoll, and H. Schulz, *Phys. Rev.* **D40**, 157 (1989).

[24] J. Cleymans, J. Stalnacke, E. Suhonen, and G.M. Weber, *Z. Phys.* **C53**, 317 (1992).

[25] J. Cleymans, M.I. Gorenstein, J. Stalnacke, and E. Suhonen, *Phys. Scripta* **48**, 277 (1993).

[26] C.M. Hung and E.V. Shuryak, *Phys. Rev. Lett.* **75**, 4003 (1995); *Phys. Rev.* **C57**, 1891 (1998).

[27] S.A. Bass and A. Dumitru, *Phys. Rev.* **C61**, 064909 (2000).

[28] E.G. Nikonov, A.A. Shanenko, and V.D. Toneev, *Heavy Ion Phys.* **8**, 89 (1998); Yad. Fiz. **62**, 1301 (1999) [translated as Physics of Atomic Nuclei, **62**, 1226 (1999)].

[29] V.D. Toneev, E.G. Nikonov, and A.A. Shanenko, in *Nuclear Matter in Different Phases and Transitions*, eds. J.-P. Blaizot, X. Campi, and M. Ploszajczak, Kluwer Academic Publishers (1999), p.309.

[30] M. I. Gorenstein and S. N. Yang, *Phys. Rev.* **D52**, 5206 (1995); *ibid, J. Phys.* **G21**, 1053 (1995).

[31] T.S. Biro, A.A. Shanenko and V.D. Toneev, Yad. Fiz. **66**, 1015 (2003) [translated as Physics of Atomic Nuclei, **66**, 982 (2003)]; nucl-th/0102027.

[32] L.D. Landau and E.M. Lifshitz, *Statistical Physics*, vol.5, Part 1, Pergamon Press, 1980.

[33] N. Glendenning, *Phys. Rev.* **D46**, 1274 (1992); *Phys. Rep.* **342**, 393 (2001).

[34] J. Cleymans, R.V. Gavai and E. Suhonen, *Phys. Rep.* **130**, 217 (1986); J. Cleymans, K. Redlich, H. Satz and E. Suhonen, *Z. Phys.* **C58**, 347 (1993).

[35] U. Heinz, P.R. Subramanian, H. Stöcker, and W. Greiner, *J. Phys.* **G12**, 1237 (1986); J. Cleymans, K. Redlich, H. Satz, and E. Suhonen, *Z. Phys.* **C33**, 151 (1986); E. Suhonen and S. Sohlo, *J. Phys.* **G13**, 1487 (1987); H. Kuono and F. Takagi, *Z. Phys.* **C42**, 209 (1989); J. Cleymans and E. Suhonen, *Z. Phys.* **C37**, 51 (1987); J. Cleymans, H. Satz, E. Suhonen, and D.W. von Oertzen, *Phys. Lett.* **B242**, 111 (1990).

[36] D.H. Rischke, M.I. Gorenstein, H. Stöcker, and W. Greiner, *Z. Phys.* **C51**, 485 (1991).

[37] J. Zimanyi et al., *Nucl. Phys.* **A484**, 647 (1988).

[38] N. Prasad, K.K. Singh and C.P. Singh, Phys. Rev. **C62**, 037903 (2001).

[39] E.G. Nikonov, A.A. Shanenko and V.D. Toneev, Heavy Ion Phys. **4**, 333 (1996).

[40] K. Redlich and H. Satz, *Phys. Rev.* **D33**, 3747 (1986).

[41] V.D. Toneev, N.S. Amelin, K.K. Gudima, and S.Yu. Sivoklokov *Nucl. Phys.* **A519**, (463c); N.S. Amelin *et al. Phys. Rev.* **C44**, 1541 (1991); N.S. Amelin *et al. Phys. Rev.* **C47**, 2299 (1993).

[42] P.R. Subramanian, H. Stöcker and W. Greiner *Phys. Lett.* **B173**, 468 (1986).

[43] J. Cleymans and K. Redlich *Phys. Rev. Lett.* **81**, 5284 (1998).

[44] R. Stock, hep-ph/0204032; The NA49 Collaboration, *Phys. Rev.* **C66**, 054902 (2002); nucl-ex/0205002; M. van Leeuwen for the NA49 Collaboration, *Nucl. Phys.* **A715**, 161 (2003); nucl-ex/02080714.

[45] J. Cleymans and K. Redlich *Phys. Rev.* **C60**, 054908 (1999).

[46] V.D. Toneev, J. Cleymans, E.G. Nikonov, K. Redlich, and A.A. Shanenko, *J. Phys.* **G27**, 827 (2001).

[47] K.A. Bugaev, *Nucl.Phys.* **A606**, 59 (1996).

[48] R. Rapp and E.V. Shuryak, *Phys. Rev. Lett.* **86**, 2980 (2001).

[49] C.M. Ko, V. Koch, Z. Lin, K. Redlich, M. Stephanov, and X.N. Wang, *Phys. Rev. Lett.* **86**, 5438 (2001).

[50] R. Hagedorn and K. Redlich, *Z. Phys.* **C27**, 541 (1985); K. Redlich and L. Turko, *Z. Phys.* **C5**, 201 (1980).

[51] J. Cleymans, K. Redlich and E. Suhonen, *Z. Phys.* **C51**, 137 (1991).

[52] We thank P. Braun–Munzinger for pointing out this issue.

[53] K. Redlich, *Nucl. Phys.* **A698**, 94 (2002); hep-ph/0105104.

[54] P. Braun-Munzinger, J. Cleymans, H. Oeschler, and K. Redlich, *Nucl. Phys.* **A697**, 902 (2002); hep-ph/0105104.

[55] K. Wròblewski, *Acta Phys. Polon.* **B16**, 379 (1985).

[56] M. Gazdzicki, hep-ph/0305176.